Available online at www.sciencedirect.com
ScienceDirect
Surface Science 601 (2007) 699–705
SURFACE SCIENCE
www.elsevier.com/locate/susc

Structure, magnetism, and adhesion at Cr/Fe interfaces from density functional theory

Donald F. Johnson [a], D.E. Jiang [b], Emily A. Carter [c,*]

[a] Department of Chemistry, Princeton University, Princeton, NJ 08544, USA
[b] Oak Ridge National Laboratory P.O. Box 2008, MS-6201, Oak Ridge, TN 37831, USA
[c] Department of Mechanical and Aerospace Engineering and Program in Applied and Computational Mathematics, Princeton University, Princeton, NJ 08544-5263, USA

Received 7 July 2006; accepted for publication 27 October 2006
Available online 15 November 2006

Abstract

Properties of the Cr(100)/Fe(100) and Cr(110)/Fe(110) interfaces are investigated with spin-polarized density functional theory within the generalized gradient approximation (DFT-GGA) for electron exchange and correlation. Contrary to earlier predictions for a monolayer of Cr on bulk Fe, we find intermixing of Cr and Fe at the interface of thick films to be endothermic; hence here we focus on characterizing abrupt, unalloyed interfaces. The ideal work of adhesion for both the (100) and (110) abrupt interfaces is predicted to be $\sim$5.4 J/m^2. We propose that this anomalously strong adhesion between heterogeneous interfaces is derived from significant spin correlations and d–d bonding at the interface.

Keywords: Metal–metal magnetic thin film structures; Metal–metal interfaces; Density functional calculations; Adhesion; Iron; Chromium; Coatings

1. Introduction

Chromium is used as a protective coating on steel in many areas of industry due to its high melting point and wear resistance. For example, steel gun barrels are subjected to extreme operating conditions during firing, such as high pressures, high temperatures, mechanical stresses, and corrosive blast gases [1]. Steel alone will erode rather quickly under these conditions and alloying the steel is not enough to withstand the high temperatures and corrosive gases. Currently, the Army protects the inside of gun barrels with a thin coating of Cr. While the Cr layer provides good thermal protection and adheres strongly to steel, this coating still presents some drawbacks. The electroplating process used to deposit the Cr leaves behind small micro-cracks which allow blast gases to penetrate through, corrode the steel, and erode the interface, leading to spallation of the Cr layer [1]. This damage necessitates frequent maintenance that affects Army logistics. After spalling, the Cr is swept out of the gun tube during subsequent blasts, which leads to another problem: environmental contamination. In an oxidizing environment, Cr will eventually become Cr(VI), which leads in turn to the formation of toxic and carcinogenic chromates in the soil [2,3].

The search for potential alternative protective coatings for steel has been aimed primarily at ceramic coatings/liners (see, e.g. [4] and references therein). Ceramic/iron interfaces have been studied experimentally, e.g., alumina growth on Fe(110) [5] and MgO/Fe [6]. First principles quantum mechanics has been used by our group and others to characterize metal–carbide and metal–silicide ceramic/iron interfaces (e.g., ZrC [7], TiC [8–10], and $MoSi_2$ [11] on Fe substrates).

While ceramics are promising in terms of hardness and thermal protection potential, it is not clear whether they will bond to the steel strongly enough to withstand the

* Corresponding author. Tel.: +1 609 258 5391; fax: +1 609 258 5877.
E-mail address: eac@princeton.edu (E.A. Carter).

0039-6028/$ - see front matter © 2006 Elsevier B.V. All rights reserved.
doi:10.1016/j.susc.2006.10.034

mechanical shocks and stresses associated with the firing of a projectile. As a baseline point of comparison during the search for alternative coatings that adhere strongly to steel, it is important to investigate the very stable Cr/Fe interface currently employed, in order to discern the origin of its strong adhesion. Such insights may help in the design of less toxic, more robust, alternative coatings.

In addition to coatings applications, Cr–Fe interfaces also garner attention from the electronics industry, since the junction of ferromagnetic (FM) Fe with anti-ferromagnetic (AF) Cr exhibits giant magnetoresistance (GMR). Fe/Cr/Fe sandwiches have become a prototype system for studying this effect. Recent DFT calculations predicted that GMR in Fe/Cr/Fe sandwiches is affected by the FM layer thickness [12,13]. The magnetic ordering of Cr ultrathin films on an Fe substrate has been probed by using surface-sensitive techniques, including spin-polarized electron-energy-loss spectroscopy [14] and spin-polarized electron emission spectroscopy [15], with both probes detecting AF coupling at the interface. A monolayer of Cr on an Fe substrate has been examined using spin-polarized DFT within the generalized gradient approximation (GGA) [16,17] and the interface Green's function technique [18], with both methods predicting AF coupling of the Cr monolayer to the Fe substrate, in agreement with experiment. From a structural standpoint, DFT calculations [16,17], Auger-electron spectroscopy [19,20], and scanning tunneling microscopy [21] all have provided evidence of Cr–Fe alloy formation for ultrathin ($\leqslant$1 ML) Cr films on Fe. Semi-empirical tight-binding (SE-TB) calculations predicted Cr–Fe intermixing to be favorable in thicker ($\sim$6 ML Cr) films for certain magnetic configurations [22], but to our knowledge no first principles calculations have investigated thicker films until the present work. Epitaxial growth of Cr on Fe (0 0 1) carried out at elevated temperatures ($\sim$300 °C) does lead to intermixing, however this may be kinetically driven since such intermixing is suppressed somewhat at lower temperatures [20]. Here we employ DFT to investigate properties of both abrupt and alloyed Cr/Fe interfaces in thick films.

2. Calculational details

We performed plane-wave-based, spin-polarized periodic DFT calculations with the Vienna *ab-initio* simulation package (VASP) [23,24]. The all-electron (frozen core) Projector Augmented Wave (PAW) DFT method was employed [25,26]. The GGA of Perdew, Burke, and Ernzerhof (PBE) was utilized for the exchange-correlation functional [27]. We used the standard versions of the PAW-PBE potentials for Fe and Cr supplied with VASP. The PAW method was employed instead of a pseudopotential technique because it has been shown recently that conventional spin-neutral ultra-soft pseudopotentials (USPPs) produce the wrong ordering of some magnetic states of bulk Fe [28,29], while the PAW potentials produce the correct ordering of states. Similarly, the GGA for the electron exchange-correlation functional was used because the local density approximation (LDA) predicts the wrong ground state for Fe (hcp instead of bcc) [28,30].

We performed calculations on two bcc Cr/bcc Fe interfaces: (1 0 0)/(1 0 0) and (1 1 0)/(1 1 0). We did not consider the bcc Fe(1 1 1) surface, since it has a significantly higher surface energy and therefore is less likely to be present as a facet on a polycrystalline substrate during Cr deposition. We increased the k-point sampling for bulk and interface cells until the total energy was converged to within 5 meV/atom. For bulk Fe and Cr, we used a $15\times15\times15$ k-mesh on the primitive 2-atom bcc unit cell to obtain lattice constants and bulk magnetic moments. We used a $15\times15\times1$ k-mesh for the (1 0 0) interface, resulting in a k-point spacing of 0.1478 Å^{-1} in the periodic x- and y-directions. A k-mesh of $15\times11\times1$ was employed for the (1 1 0) interface producing a k-point spacing of 0.1478 Å^{-1} in the x-direction and 0.1425 Å^{-1} in the y-direction. The kinetic energy cutoff for the plane-wave basis was increased until the total energy was converged to within 1 meV/atom. As a result, in all calculations, we used kinetic energy cutoffs of 400 eV for the pseudowavefunctions and 511 eV (402 eV) for the Fe and Fe/Cr (pure Cr) augmentation charges.

The atoms were relaxed to within a force tolerance of 0.05 eV/Å using a conjugate-gradient algorithm. In order to obtain accurate forces, the first-order Methfessel–Paxton method [31] was used for Fermi-surface smearing with a smearing width of 0.1 eV. The error introduced in the total energy (extrapolated to 0 K) by this small smearing width is less than 1 meV/atom.

Using these parameters at the PAW-GGA level of theory, we obtain good agreement with experiment for bulk properties of FM bcc Fe and AF bcc Cr. The predicted equilibrium lattice constant for Fe is $a_0 = 2.834$ Å, the predicted bulk modulus is $B = 174$ GPa, and the predicted local magnetic moment is $\mu = 2.20\ \mu_B$. These values agree well with previous PAW-GGA results [28] and experiment ($a_0 = 2.86$ Å [32]; $B = 168$ GPa, $\mu = 2.22\ \mu_B$ [33]). The equilibrium lattice constant for bcc Cr is calculated to be 2.855 Å and the predicted bulk modulus is 190 GPa, both of which agree fortuitously well with experiment: $a_{exp} = 2.88$ Å and $B_{exp} = 191$ GPa [34]. The agreement must be considered fortuitous because the actual magnetic ground state of bcc Cr is an incommensurate AF spin-density wave (SDW), with a period of 20.83 lattice constants and amplitude $M_{exp} = 0.62\ \mu_B$ [34], which we simplified to the related AF state of bcc Cr. A first-principles calculation of the full SDW would require both a prohibitively large periodic cell as well as a non-collinear-spin DFT calculation [35–37], which is beyond the scope of this work. More importantly, when Cr is deposited on bcc Fe substrates, it is known to undergo spin ordering such that the SDW disappears and the AF Cr magnetic state becomes the preferred state [14]. Since we are primarily interested in the properties of the Fe–Cr interface, the AF state of Cr is of greater relevance. Our AF bcc Cr model has a magnetic moment of

1.09 μ_B, in agreement with previous all-electron DFT-FLAPW-GGA calculations on AF Cr: $a = 2.871$ Å, $B = 184$ GPa, and $M = 1.08$ μ_B [34].

As noted above, Fe and Cr both have bcc structures and very similar lattice parameters. Matching the interfaces together is very straightforward: Cr atoms are placed to simply continue the bcc geometry. Cr is under slight compression, but the lattice mismatch [38] is only 0.7%. Since the lattice constants of Fe and Cr are so close, a coherent interface is expected to form, where the equilibrium structure of the Fe substrate is assumed to determine the lattice parameters for the interface.

The interface model consists of a slab of Fe, a slab of Cr, and 10 Å of vacuum in a periodic unit cell, so that the periodic images of the interface slab are well separated by vacuum and will not interact. The outer half of the Fe slab is held fixed at the bulk geometry, both for the isolated Fe substrate slabs and for the interface slabs, in order to mimic a semi-infinite bulk crystal substrate. The Cr layers are all allowed to relax, both in the interface slab and the isolated slab, subject to the constraint of using Fe lattice vectors to define the unit cell, in order to mimic a thin film coating. The number of layers is incrementally increased from 4(Cr)/5(Fe) up to 12(Cr)/12(Fe) for the (1 0 0) interface and from 6(Cr)/6(Fe) to 10(Cr)/10(Fe) for the (1 1 0) interface. Generally, the number of Cr and Fe layers is increased until the ideal work of adhesion (defined below) converges, but the number of layers also should be increased until the centers of the Cr and Fe slabs resemble the bulk both structurally and electronically. This converged thickness then ensures that the Cr free surface is not affecting the interface. Specifically, one metric for determining a sufficient slab thickness is that the magnetic moments on atoms in the center of the slab should match bulk magnetic moments. Additionally, the forces between the fixed Fe atoms and relaxed Fe atoms should be small, typically less than 0.05 eV/Å, which is the same convergence criteria used for ionic relaxations.

The Cr(1 0 0)/Fe(1 0 0) interface only requires one atom per layer in the periodic supercell and the Cr layers alternate spin up/spin down, i.e., simple AF coupling [14,15]. For the (1 0 0) interface, we used slabs with an even number of layers to keep the number of spin up Cr equal to the number of spin down Cr. The magnetic periodicity of AF Cr in the Cr(1 1 0)/Fe(1 1 0) interface requires two atoms per layer such that one spin-up and one spin-down atom are present in each Cr layer. The cross-sectional areas of the (1 0 0) and (1 1 0) interface periodic cells are thus 8.032 Å^2 and 11.358 Å^2, respectively.

The ideal work of adhesion, W_{ad}, is estimated from the energy difference between the structurally relaxed interface and the separated slabs, keeping the lattice parameters fixed at those of the substrate so as to calculate a unique W_{ad}, independent of elastic strain energy contributions [39], which should be very small anyway in this case. The ideal work of adhesion is defined as $W_{ad} = (E_1 + E_2 - E_{12})/\text{Area}$, where E_{12} is the energy of the coating/substrate system, E_1 is the energy of the coating, and E_2 is the energy of the substrate. With this definition, the "intrinsic adhesion" of a pure material, say Fe, is simply twice the surface energy, $2\gamma_{surf}$.

In order to calculate the magnetic moment μ on a specific atom, the charge density for each spin component is integrated within a sphere centered on the atom and the difference gives μ. The radii of the spheres are the standard Wigner–Seitz values supplied by VASP for each ionic species: 1.302 Å for Fe and 1.323 Å for Cr. The calculations were started with each Fe in a fully FM state ($\mu = 4$ μ_B) and each Cr in a fully AF state ($\mu = \pm 6$ μ_B), with some exceptions. In the Cr(1 1 0) slab calculations, the system would often relax to a higher energy, metastable magnetic state. Breaking the symmetry by starting certain atoms at $\mu = \pm 5$ μ_B helped most systems find the AF ground state, but despite many attempts, we were unable to relax the 10-layer Cr(1 1 0) slab to the true magnetic ground state.

3. Results and discussion

In what follows, we refer to Fe_{surf} as the Fe atom at the free surface and Fe_{int} as the Fe atom at the interface; likewise for Cr_{surf} and Cr_{int}.

3.1. Structures of the Cr(1 0 0)/Fe(1 0 0) and Cr(1 1 0)/Fe(1 1 0) interfaces

For both interfaces, we find very slight structural relaxations in the interior of each material, while reduced interlayer spacings are observed at interfaces and surfaces. The distances between (1 0 0) planes are 1.417 Å and 1.428 Å in bulk Fe and Cr, respectively, while the inter-planar (1 1 0) separations are 2.00 Å (2.02 Å) for bulk Fe (Cr).

In the relaxed (1 0 0) interface slab, the layer spacings are all within 1% of the bulk values, except near the interface itself and at the free Cr surface. The Cr surface layer is 1.35 Å from the subsurface layer for all layer thickness considered, corresponding to about 5% inward relaxation. As the total number of layers increases, the Fe_{int}–Cr_{int} distance decreases slightly from 1.41 Å to 1.38 Å. This interlayer distance is shorter than in either pure metal, suggestive of strong heterometallic bonding.

The structure of the (1 1 0) interface again exhibits some shortening of interlayer spacings at the interface itself and the Cr surface and small changes elsewhere. For the thickest films, the Fe_{int}–Cr_{int} interplanar distance is 1.98 Å, again slightly decreased compared to the pure elements. The Cr surface atoms in all films again relax inward, by −0.02 Å, or 1%. Buckling of Cr atoms is negligible, i.e., there is no difference (<0.01 Å) between the Fe(↑)–Cr(↓) distance and the Fe(↑)–Cr(↑) distance in all films considered. Overall, the relaxations at the (1 1 0) interface are less pronounced compared to the (1 0 0) interface.

Both theory and experiment have investigated intermixing at the Cr/Fe interface, which occurs for (sub)monolayer Cr films on Fe(1 0 0), resulting in the formation of,

e.g., $Fe_{50}Cr_{50}$ surface alloys [16,17,19]. We considered formation of such interface alloys in our thick films, but determined that at zero Kelvin they are less stable than sharp, unalloyed Fe/Cr interfaces. Swapping half the Cr_{int} atoms with Fe_{int} atoms (to create two layers of ordered $Fe_{50}Cr_{50}$) increased the Fe(100)/Cr(100) interfacial energy significantly. In a 2×2 interface cell, with four atoms per layer, five unique ways exist to swap interface atoms (taking symmetry into account) and all five configurations were less stable than an abrupt interface by $\geqslant 0.25\ J/m^2$. Likewise, we found that swapping Cr_{int} atoms with Fe_{int} atoms at the Fe(110)/Cr(110) interface was even less favorable by at least $1.09\ J/m^2$ compared to the abrupt interface. Here we considered the two configurations possible in the 1×1 interface cell.

The lowest energy magnetic states found for these metastable alloy films were consistent with previous DFT-GGA [16] and SE-TB [22] calculations, namely the Cr atoms in the first alloy layer (Fe side) were spin-down while the Cr atoms in the second alloy layer (Cr side) were spin-up, when all Fe atoms were ferromagnetically coupled spin-up. This held for both the (100) and (110) alloy interfaces. Cr atoms in the (100) and (110) alloy interfaces had similar spins to those in the abrupt (100) or (110) interfaces, respectively.

The surface alloy is known to form during elevated temperature epitaxial *monolayer* growth of Cr on the Fe (100) surface [19–21], but it is not known whether an interface alloy would form during the room temperature electroplating process typically used to deposit chrome coatings on steel. Bulk alloy thermodynamics, applicable for macroscopically thick Cr coatings on steel, does not necessarily apply to ultrathin films, a regime where metastable alloy phases often form [40]. Our results are meant to model bulk Cr coatings on bulk Fe substrates, where we find alloying is disfavored compared to sharp interfaces between the two metals, in contrast to previous semi-empirical calculations [22]. Kinetically driven intermixing during epitaxial growth may leave the system in a metastable alloyed state at the interface after the growth of many layers, but an abrupt interface may still be the global minimum and may be the one formed during room temperature processing.

3.2. Adhesion for Cr(100)/Fe(100) and Cr(110)/Fe(110)

Fig. 1 shows the ideal work of adhesion W_{ad} as a function of the number of Cr and Fe layers in the slab model. The adhesion energy converges (within 1%) to a value of $5.37\ J/m^2$ for the (100) interface and $5.35\ J/m^2$ for the (110) interface. This is intermediate between Fe–Fe and Cr–Cr cohesion, i.e., greater than the predicted intrinsic adhesion $[2\gamma_{surf}(110)]$ of Fe of $4.8\ J/m^2$, but less than the predicted intrinsic adhesion of Cr, $[2\gamma_{surf}(110)] = 6.28\ J/m^2$. The value is slightly smaller than predicted by a linear interpolation of the intrinsic adhesion energies of the pure elements. The 10-layer Cr (110) slab could not be converged to the ground magnetic state; therefore the W_{ad} value resulting from the 10(Fe)–10(Cr) interface calculation is unreliable and not reported. We find little variability in the (110) interface W_{ad} as the slab thickness is increased, while the (100) interface W_{ad} varies up to 6% going from 4 to 12 layers of Cr/Fe.

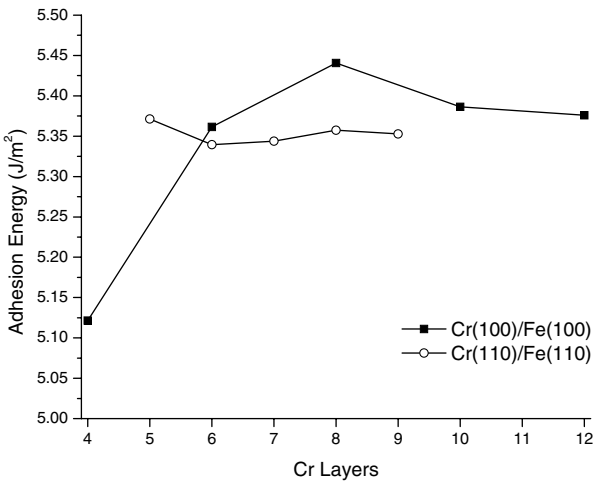

Fig. 1. Convergence of the ideal work of adhesion (W_{ad}) vs. layer thickness: Cr(100)/Fe(100) (squares); Cr(110)/Fe(110) (circles).

The calculations for W_{ad} may be considered upper bounds to the ideal work of adhesion, since the cleaved Cr slab is held fixed to the original bulk Fe lattice parameters and the atoms are relaxed within this constraint. It is, of course, not a true upper bound to the actual adhesion energy, since plasticity has been neglected, as it must be for such small model systems. However, trends in the ideal adhesion strengths and comparisons to intrinsic adhesion in bulk materials may still be useful indicators of the relative stability of such interfaces.

3.3. Bonding at the interface

Fig. 2(a) presents the angular-momentum-resolved local density of states (LDOS) projected onto various atoms at the (100) interface. The s and p states are combined into one thin line for each element. Substantial population at the Fermi level indicates metallic bonding plays a role at the interface. However, the strong overlap of both bonding ($<\varepsilon_F$) and antibonding ($>\varepsilon_F$) Cr and Fe d states suggests covalent d–d bonding is likely responsible for the strong adhesion calculated. In particular, the significant overlap of majority (α) spin Fe states with majority (β) spin Cr states suggests antiferromagnetic coupling of Cr to Fe at the interface produces strong d–d bonding.

Fig. 2(b) and (c) display the LDOS for spin up Cr (and coplanar Fe) and spin down Cr (and coplanar Fe), respectively. These two groups are illustrated in Fig. 3 as atoms labeled **a** (spin up Cr) and **b** (spin down Cr). The two profiles are very similar, but the DOS at the Fermi level have different magnitudes in each case. The Fe and Cr sp states at both interfaces are highly dispersed, indicative of metallic bonding. The increased LDOS at ε_F for the Cr

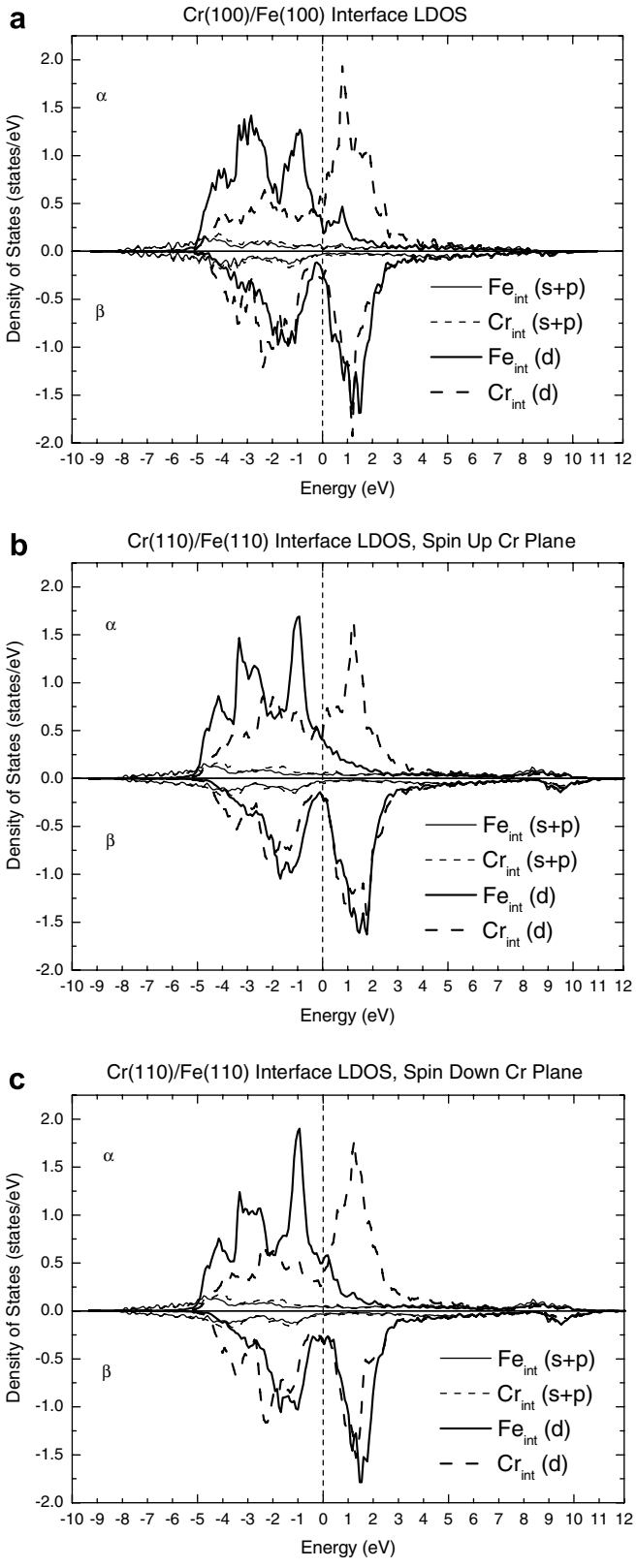

Fig. 2. Spin-polarized projected local density of states for: (a) Cr and Fe at the (100) interface, (b) spin up Cr and coplanar Fe at the (110) interface (group A in Fig. 3), (c) spin down Cr and coplanar Fe at the (110) interface (group B in Fig. 3). Solid lines correspond to Fe LDOS and dashed lines correspond to Cr LDOS. The s- and p-states are summed for each element and shown as one thin DOS line. The α-spin (β-spin) LDOS are shown as positive (negative) values. The Fermi level is at 0 eV.

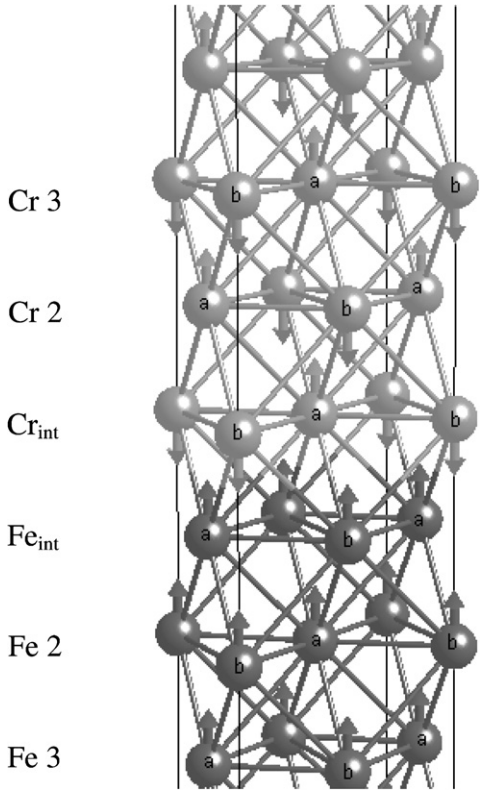

Fig. 3. Magnetic structure of the (110) interface, displaying two groups of atoms: group A consists of spin-up Cr atoms and coplanar Fe atoms; group B consists of spin-down Cr and coplanar Fe atoms. Atoms in a given group lie in the same (100) plane perpendicular to the interface.

spin-down (AF) case suggests stronger metallic Cr–Fe bonding compared to the FM spin coupling plane. Covalent d–d bonding is again evidenced by a strong overlap of Cr and Fe d states above and below the Fermi level.

3.4. Magnetism for Cr(100)/Fe(100) and Cr(110)/Fe(110)

Fig. 4(a) displays the calculated magnetic moment of the atoms in each layer of the (100) interface. In the 12-layer/12-layer interface, the magnetic moment at the center of the Fe slab is 2.2 μ_B and at the center of the Cr slab it is $=\pm 0.98\ \mu_B$. This close agreement to bulk magnetic moments indicates that the magnetic properties are converged with respect to slab thickness. The magnetic moments at the center of the Cr slabs are slightly smaller than the bulk magnetic moments because of lattice cell compression. When the properties of bulk Cr are calculated at the bulk Fe lattice constant, we obtain $\mu = \pm 0.95\ \mu_B$ for Cr instead of $\pm 1.09\ \mu_B$ found in the equilibrium bulk structure of bcc Cr. We therefore do not expect M_{Cr} to approach 1.09 μ_B as more layers are added. The magnetic moments of the atoms at the surface (Fe_{surf}, Cr_{surf}) are larger than in the bulk or interface due to under-coordination of the metal atoms, which allows the spin magnetic moment to move toward the high spin moment of the free atom. The magnetic

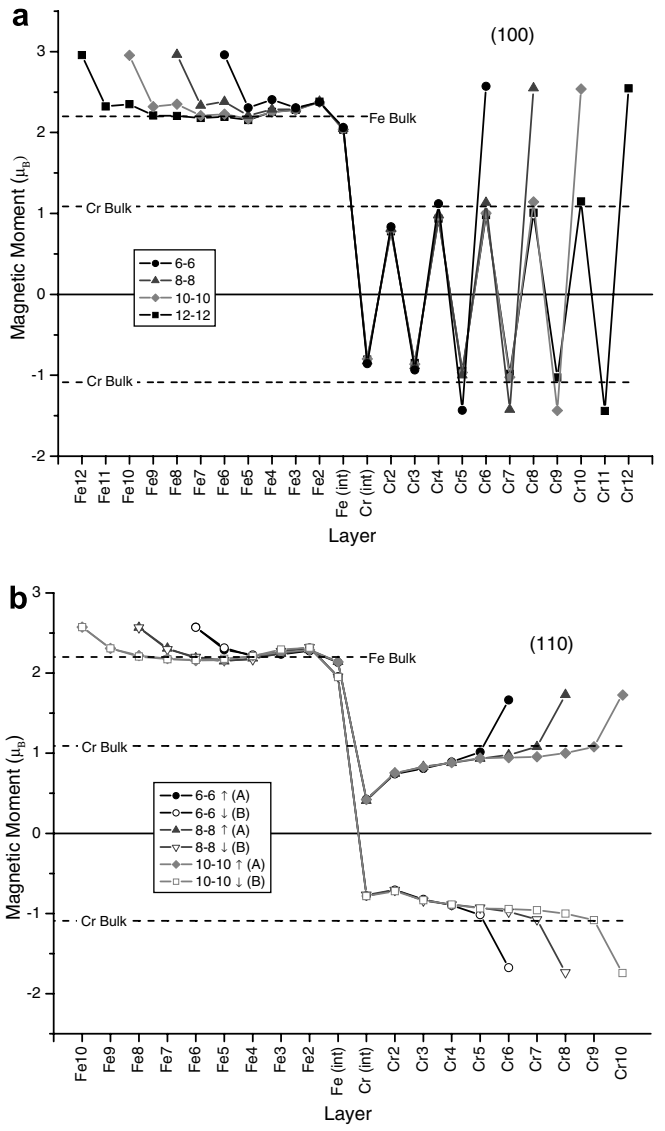

Fig. 4. Layer-resolved magnetic moments of: (a) Cr(100)/Fe(100), 6 layer–6 layer interface (circles), 8–8 (triangles), 10–10 (diamonds), and 12–12 (squares); (b) Cr(110)/Fe(110) 6–6 (circles), 8–8 (triangles), and 10–10 (squares); solid shapes correspond to atoms in group A (spin up Cr plane) and open shapes correspond to atoms in group B (spin down Cr plane). See Fig. 3.

moments of the interface atoms (Fe_{int}, Cr_{int}) deviate from their bulk values, as discussed in detail later. Overall, the magnetic moments of Fe_{int}, Cr_{int}, Fe_{surf}, and Cr_{surf} change very little as the total number of layers increases from 12 to 24, suggesting that the magnetic properties for this interface converge rapidly with distance away from the interface.

Fig. 4(b) displays the magnetic moment of the atoms in each layer of the (110) interface. For each interface, two lines are plotted: solid shapes correspond to the plane with spin-up Cr atoms (see Fig. 3, group A) and open shapes to the plane with spin-down Cr atoms (see Fig. 3, group B). These are (001) planes perpendicular to the interface plane, as illustrated in Fig. 3. Note that atoms in the same group are not nearest neighbors, e.g., Fe_{int}(b) atoms coplanar with spin-down Cr atoms are not nearest neighbors to the spin-down Cr_{int}(b) atoms. They are closer to the spin-up Cr_{int}(a) atoms, but still exhibit strong correlation with the spin-down Cr. In Fig. 4(b), we can see that the Fe_{int}(b) has a smaller magnetic moment than the Fe_{int}(a) in all three cases. The Fe_{int}(b) atoms are attempting to reduce the AF coupling by reducing their magnetic moments, while the latter Fe_{int}(a) are quite happily FM coupled to the Cr_{int}(a) atoms and retain their large magnetic moments. Again, the magnetic behavior at the centers of the Fe/Cr slabs is very bulk-like. In the 10-layer/10-layer interface, the Cr atoms in the 5th, 6th, and 7th layers away from the interface all have magnetic moments very close to M_{bulk}, which indicates again that the finite slab's properties are converged with respect to number of atomic layers. As layers are added, the magnetic moment of Cr_{surf} increases slightly, while the interface atoms remain unchanged.

At both (100) and (110) interfaces, the magnetic moment of Fe_{int} is less "spin up" than expected for pure Fe, due to its interaction with the neighboring Cr atoms, which have smaller magnetic moments than Fe. Similarly, Cr_{int} atoms are more spin-down-like than expected due to the large spin moment on nearby Fe_{int} atoms and the preference of Cr for AF coupling. The (110) Cr_{int}(b) atoms have increased spin-down moments, while (110) Cr_{int}(a) atoms have decreased spin-up moments. The magnitude of Cr magnetic moments, $|\mu|$, generally decreases from the free surface towards the interface. The strong magnetic interaction leads to the shorter interfacial distance and enhanced bonding. The spin pairing at these interfaces is likely to be the origin of the enhanced bonding compared to pure Fe, while the magnetic frustration of the Fe that experiences AF coupling with the spin-down Cr atoms at the interface [Cr_{int} atoms in (100) and Cr_{int}(b) atoms in (110)] may explain why the cohesion is weaker than in pure Cr.

4. Conclusions

First principles PAW-DFT-GGA calculations were performed for Cr/Fe interfaces. We find no tendency to form an interface alloy in these thick films at low temperatures relevant for room temperature electroplating of chrome on steel. Both the (100) and (110) interfaces show very strong adhesion, with the electronic structure suggesting strong covalent d–d bonding in addition to metallic cohesion. This strong interfacial bonding is evidenced by strong spin correlations and a decrease in the expected Cr–Fe interfacial distance. It will be a significant challenge to find an alternative thin film coating to Cr given its extraordinary stability due to the strong spin correlations and the nearly complete lack of strain due to the excellent lattice matching between Fe and Cr. However, it suggests that coatings that maximize a mixture of localized covalent and delocalized metallic bonding should be the type of material on which to focus. Our current research follows this design principle.

Acknowledgements

This work was supported by a grant from the Army Research Office. Computations were performed on IBM NH-2 SMP P3 machines at the ARL MSRC in Maryland.

References

[1] P.J. Cote, C. Rickard, Wear 241 (2000) 17.
[2] D. Blowes, Science 295 (2002) 2024.
[3] A.S. Ellis, T.M. Johnson, T.D. Bullen, Science 295 (2002) 2060.
[4] R.H. Carter, J. Pressure Vessel Tech. 128 (2006) 251.
[5] Y.S. Dedkov, M. Fonin, U. Rudiger, G. Guntherodt, Appl. Phys. Lett. 81 (14) (2002) 2584.
[6] J. Faupel, C. Fuhse, A. Meschede, C. Herweg, H.U. Krebs, S. Vitta, Appl. Phys. A 79 (2004) 1233.
[7] A. Arya, E.A. Carter, Surf. Sci. 560 (2004) 103.
[8] A. Arya, E.A. Carter, J. Chem. Phys. 118 (2003) 8982.
[9] J.H. Lee, T. Shishidou, Y.-J. Zhao, A.J. Freeman, G.B. Olson, Phil. Mag. 85 (2005) 3683.
[10] M. Mizuno, I. Tanaka, H. Adachi, Acta Mater. 46 (1998) 1637.
[11] D.E. Jiang, E.A. Carter, Acta Mater. 53 (2005) 4489.
[12] M. Pereiro, D. Baldomir, S. Man'kovsky, J. Arias, Int. J. Quantum Chem. 91 (2003) 245.
[13] M. Pereiro, J. Botana, D. Baldomir, K. Warda, L. Wojtczak, S.V. Man'kovsky, M. Iglesias, V. Pardo, J.E. Arias, J. Magn. Magn. Mater. 290–291 (2005) 392.
[14] T.G. Walker, A.W. Pang, H. Hopster, S.F. Alvarado, Phys. Rev. Lett. 69 (1992) 1121.
[15] R. Pfandzelter, M. Ostwald, H. Winter, Phys. Rev. B 63 (2001) 140406.
[16] H.C. Herper, E. Hoffman, P. Entel, Phase Transit. 75 (2002) 185.
[17] A. Kellou, H. Aourag, Phys. Status Solidi (B) 236 (2003) 166.
[18] S. Mirbt, O. Eriksson, B. Johansson, H.L. Skriver, Phys. Rev. B 52 (1995) 15060.
[19] R. Pfandzelter, T. Igel, H. Winter, Phys. Rev. B 54 (1996) 4496.
[20] D. Venus, B. Heinrich, Phys. Rev. B 53 (1996) R1773.
[21] A. Davies, J.A. Stroscio, D.T. Pierce, R.J. Celotta, Phys. Rev. Lett. 76 (1996) 4175.
[22] I. Turek, M. Freyss, P. Weinberger, D. Stoeffler, H. Dreyssé, Phys. Rev. B 63 (2000) 024413.
[23] G. Kresse, J. Furthmüller, Comput. Mater. Sci. 6 (1996) 15.
[24] G. Kresse, J. Furthmüller, Phys. Rev. B 54 (1996) 11169.
[25] P.E. Blöchl, Phys. Rev. B 50 (1994) 17953.
[26] G. Kresse, J. Joubert, Phys. Rev. B 59 (1999) 1758.
[27] J.P. Perdew, K. Burke, M. Ernzerhof, Phys. Rev. Lett. 77 (1996) 3865.
[28] D.E. Jiang, E.A. Carter, Phys. Rev. B 67 (2003) 214103.
[29] V. Cocula, C.J. Pickard, E.A. Carter, J. Chem. Phys. 123 (2005) 214101.
[30] E.G. Moroni, G. Kresse, J. Hafner, J. Furthmüller, Phys. Rev. B 56 (1997) 15629.
[31] M. Methfessel, A.T. Paxton, Phys. Rev. B 40 (1989) 3616.
[32] M. Acet, H. Zähres, E.F. Wasserman, W. Pepperhoff, Phys. Rev. B 49 (1994) 6012.
[33] C. Kittel, Introduction to Solid State Physics, Seventh ed., Wiley, New York, 1996.
[34] S. Cottenier, B. De Vries, J. Meersschaut, M. Rots, J. Phys.: Condens. Matter 14 (2002) 3275.
[35] J. Kübler, K.-H. Höck, J. Sticht, A.R. Williams, J. Phys. F 18 (1988) 469.
[36] M. Freyss, D. Stoeffler, H. Dreyssé, J. Appl. Phys. 81 (1997) 4363.
[37] T. Oda, A. Pasquarello, R. Car, Phys. Rev. Lett. 80 (1998) 3622.
[38] A. Christensen, E.A.A. Jarvis, E.A. Carter, in: R.A. Dressler, C. Ng (Eds.), Chemical Dynamics in Extreme Environments, Advanced Series in Physical Chemistry, vol. 11, World Scientific, Singapore, 2001, p. 490.
[39] A. Christensen, E.A. Carter, J. Chem. Phys. 114 (2001) 5816.
[40] D.P. Woodruff (Ed.), Surface Alloys and Alloy Surfaces, The Chemical Physics of Solid Surfaces, vol. 10, Elsevier, Amsterdam, 2002.